

A 14 The numerical renormalization group for quantum impurity models

T. A. Costi

Institut für Festkörperforschung

Forschungszentrum Jülich GmbH

Contents

1	Introduction	2
2	Quantum impurity models	3
3	Wilson's numerical approach	7
4	Calculation of physical properties	12
5	Recent developments	17
6	Summary	21
A	Lanczos procedure	21
B	Logarithmic discretization approximation	22

1 Introduction

This lecture deals with a particular implementation of the renormalization group (RG) idea: Wilson's non-perturbative numerical renormalization group (NRG) method for quantum impurity models [1]. The method was originally developed in the context of the Kondo model of magnetic impurities (such as Fe or Mn) in non-magnetic metals (such as Cu, Au, Ag etc), whose Hamiltonian is given by

$$H_{KM} = \sum_{k,\mu} \varepsilon_{k,\mu} c_{k,\mu}^\dagger c_{k,\mu} + J \vec{S} \cdot \vec{s}_0 \quad (1)$$

Here, \vec{S} represents the spin of the impurity (taken here to be a $S = 1/2$ for simplicity), $\vec{s}_0 = f_{0,\mu}^\dagger \vec{\sigma}_{\mu\nu} f_{0,\nu}$, with repeated indices $\mu, \nu = \uparrow, \downarrow$ summed over, is the conduction electron spin-density at the impurity site with $f_{0,\mu} = \sum_k c_{k,\mu}$ the local Wannier state. The model (1) describes a $S = 1/2$ local moment interacting antiferromagnetically ($J > 0$) with the conduction electron spin-density at the impurity. The first term represents the kinetic energy, $\varepsilon_{k,\mu}$, of non-interacting conduction electrons with half-bandwidth D and Fermi level ϵ_F .

Before describing the specific RG transformation used by Wilson to solve the quantum mechanical many-body problem represented by (1), it is useful to outline the general idea of the RG for quantum mechanical systems. Consider a system described by a Hamiltonian $H[K]$, depending on a set of interaction parameters or coupling constants $K = (K_1, K_2, \dots)$. In the case of the Kondo model, (1), there is initially only a single coupling constant $K_1 = J$. Starting from the bare Hamiltonian, $H[K]$, one constructs a sequence of effective Hamiltonians, H_N , $N = 1, 2, \dots$, describing the physics on successively lower energy scales ω_N , $N = 1, 2, \dots$ with $\omega_1 > \omega_2 > \dots$. For example, in the case of the Kondo model, one could construct an effective Hamiltonian by integrating out conduction electron degrees of freedom close to the band edges $\pm D$ so that the new effective Hamiltonian has a reduced band-width $D' = D - \delta D$. This repeated process of integrating out high energy degrees of freedom, will lead, however, to effective Hamiltonians with additional interactions, not present in previous effective Hamiltonians. In addition, the existing interactions or couplings will acquire renormalized values K' . The renormalization group transformation, R , relates the effective Hamiltonians on successive energy scales, $H_{N+1} = R[H_N]$, or, equivalently, it relates the new to the old effective couplings, $[K_{N+1}] = R[K_N]$. As one is interested, in particular, in scale invariant behaviour, one actually works with rescaled effective Hamiltonians, $\bar{H}_N = H_N/\omega_N$, and dimensionless or rescaled couplings (defined via the \bar{H}_N). An important concept in the RG is that of fixed points: $\bar{H}^* = R[\bar{H}^*]$. In the course of the RG flow, the system may pass several unstable fixed points before reaching its ground state fixed point in the limit $N \rightarrow \infty$. In the vicinity of fixed points, the effective Hamiltonians usually take a simple form, with the deviations representing interactions which can be either relevant (if they increase under R), irrelevant (if they decrease under R) or marginal (if to linear order they are unchanged under R). Of particular interest is the ground state fixed point and the leading irrelevant deviations about it. The ground state fixed point tells us about the nature of the low energy excitation spectrum, the kind of “quasi-particles” present and what quantum numbers they carry. The leading irrelevant deviations about this fixed point describe interactions between quasi-particles [1–3].

The difficulty of this “RG program”, for a quantum mechanical system, is to have a sufficiently accurate RG transformation in order to obtain the eigenvalues and eigenstates on all energy

scales, from high energies down to the ground state. In an early analytic implementation of the RG idea [4], Anderson calculated R perturbatively in the initially small dimensionless coupling $\tilde{J} = J/D \ll 1$ - the so called “Poor Man’s” scaling approach. The calculation showed that the running coupling \tilde{J} increased with decreasing energy or increasing N . Clearly, once $\tilde{J} \sim \mathcal{O}(1)$, this approach is no longer valid and so cannot pinpoint the nature of the ground state of the Kondo model. Wilson’s breakthrough was to succeed in constructing an accurate RG transformation for the Kondo model which did not use perturbation theory in any running coupling. This allowed a quantitative description of the crossover from the weak coupling behaviour at high energies (corresponding to a free spin with unstable fixed point at $\tilde{J} = 0$) to the strong-coupling behaviour at low energies (corresponding to a fixed point with $\tilde{J} = \infty$). Effectively, at low energies, the impurity spin is bound into a “many-body singlet” involving all the electrons in the system.

The outline of this lecture is as follows: quantum impurity models are introduced in Sect. 2 and the Anderson impurity and Kondo models are described. The formal mapping of these models onto one dimensional models in k -space is outlined. Wilson’s NRG method is described in Sect. 3, where we also indicate the relation between this method and the real-space RG approaches for critical phenomena and the DMRG approach for 1-d quantum lattice models. The latter is described in detail in the lecture of Schollwöck in this book. The application of the NRG to thermodynamics, dynamics and transport properties is described in Sect. 4. An outline of some recent developments using the NRG is given in Sect. 5, and, Sect. 6 summarizes with possible future directions.

2 Quantum impurity models

Quantum impurity models describe systems where the many-body interaction (usually a Coulomb or exchange interaction) acts at a single site, the “impurity”, and the impurity is coupled to a large system, the heat bath, consisting of a macroscopically large number of non-interacting particles. These particles can be either bosons (e.g. phonons, magnons, particle-hole pairs etc) or fermions (e.g. electrons in the conduction band). The “impurity” may be a real impurity, such as Fe impurities in Au, or a two-level atom coupled to the electromagnetic field, or, just a confined region behaving like an artificial atom, as in the case of quantum dots. It may also simply represent the lowest two quantum mechanical states of a system with a double-well potential, as in the case of quantum tunneling between macroscopic fluxoid states in a superconducting quantum interference device. The transfer of electrons between donor and acceptor molecules in photosynthesis and other biological processes may also be approximately described in terms of a two-state system coupled to environmental degrees of freedom. Concrete models describing the above situations go under the names of (isotropic and anisotropic) single and multi-channel Kondo models, the Anderson impurity model and the dissipative two-state system [5]. They describe a large number of physical systems of current experimental and theoretical interest. Quantum impurity models are also of relevance in the study of correlated lattice models, since the latter are often well approximated, via the dynamical mean field theory, by a local impurity model embedded in a medium which has to be determined self-consistently – see lecture by Liebsch.

Interest in quantum impurities arose when magnetic impurities were found to be present, albeit

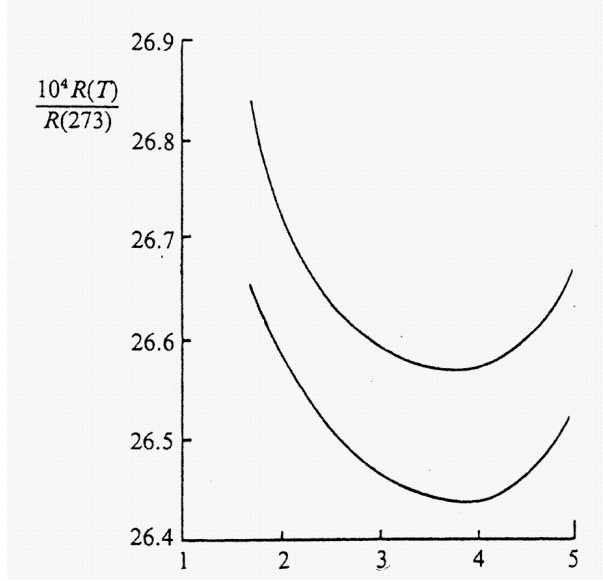


Fig. 1: Resistivity minimum in two samples of “pure” Au [6]. The expected behaviour of the resistivity for a pure metal with some weak static disorder is a T^5 term due to phonons and a saturation to a constant value, ρ_0 , at $T = 0$ due to static disorder. The former is seen in the experiment, but at low temperature an additional logarithmically increasing contribution is also found.

in very low concentrations, even in apparently very pure metals such as Au or Ag. In particular, measurements of the resistivity of Au as early as the 1930’s showed an unexpected minimum at low temperature (Fig. 1). The puzzle of the resistivity minimum was resolved by Kondo in 1964, who showed that a small concentration c_{imp} of *magnetic* impurities modelled by (1) gives rise to an additional temperature dependent term in the resistivity of the form $\rho_K = -c_{imp} b \ln(T/D)$, which increases with decreasing temperature. The balance between the decreasing phonon contribution and the increasing Kondo contribution gives rise to the observed resistivity minimum. The logarithmic contribution to the resistivity, found by Kondo in perturbation theory, cannot hold down to $T = 0$ as the total scattering remains finite in this limit (unitarity limit). Wilson’s non-perturbative NRG provides a way to obtain the correct behaviour of the resistivity also at low temperature (see Fig. 9). The next section describes the first step in this procedure for the Anderson and Kondo impurity models.

Anderson and Kondo impurity models: linear chain form

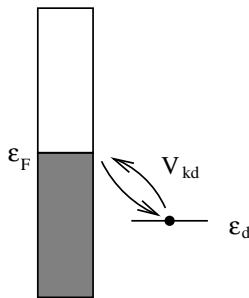


Fig. 2: Schematic representation of the Anderson impurity model. Conduction electrons in Bloch states $|k\rangle$ hybridize with an impurity level, ε_d , below the Fermi level, ε_F , of a partially filled conduction band (shaded region). The strength of the hybridization matrix elements is V_{kd} and the Coulomb repulsion on the impurity level is U . The impurity is singly occupied and behaves like a Kondo spin $S = 1/2$ when the empty and doubly occupied states are prohibited, i.e. provided $\varepsilon_d \ll \varepsilon_F$ and U is sufficiently large.

The Anderson impurity model [3] is the prototype model of strongly correlated impurity systems. This was introduced in [7] as a microscopic model for local moment formation in non-

magnetic metals. Its Hamiltonian, represented in Fig. 2, is given by

$$H_{AM} = \varepsilon_d n_d + U n_{d\uparrow} n_{d\downarrow} + \sum_{k,\mu=\uparrow,\downarrow} (V_{kd} c_{k\mu}^+ d_\mu + H.c.) + \sum_{k,\mu=\uparrow,\downarrow} \varepsilon_k c_{k\mu}^+ c_{k\mu} \quad (2)$$

The first two terms describe the impurity, which, for simplicity, is represented here by a non-degenerate s-level of energy ε_d . Electrons in the local level are subject to a Coulomb repulsion U which acts between spin-up and spin-down electrons. The local level hybridizes with the Bloch states of a non-interacting s-wave conduction band, the last term in H_{AM} , with amplitude V_{kd} . The properties of the model are determined by the hybridization function

$$\Delta(\omega) = \pi \sum_k |V_{kd}|^2 \delta(\omega - \varepsilon_k), \quad (3)$$

which, like the conduction density of states $\rho(\omega) = \sum_k \delta(\omega - \varepsilon_k)$, will in general be a complicated function of energy. In cases where the interest is in the very low energy physics, it is a good approximation to set $\Delta(\omega) \approx \Delta(\varepsilon_F) \equiv \Delta$. In applications to pseudogap systems [8] or to effective quantum impurities in dynamical mean field theory, the full frequency dependence has to be retained.

For a numerical treatment, it is useful to reformulate the Anderson model in the form of a linear chain model [9]. This allows the model to be iteratively diagonalized by a procedure to be described in Sect. 3. We first notice that the impurity state in the Anderson model hybridizes with a local Wannier state $|0, \mu\rangle = f_{0,\mu}^+ |\text{vac}\rangle$, with $|\text{vac}\rangle$ the vacuum state, and $f_{0,\mu}^+$ given by

$$V f_{0,\mu}^+ = \sum_k V_{kd} c_{k,\mu}^+. \quad (4)$$

The value of V follows from the normalization $\{f_{0,\mu}, f_{0,\mu}^+\} = 1$

$$V = (\sum_k |V_{kd}|^2)^{1/2}. \quad (5)$$

Using the above local state one can apply the Lanczos procedure (Appendix A) for tridiagonalizing a Hermitian operator, such as H_c , to obtain

$$H_c = \sum_{k,\mu} \varepsilon_k c_{k,\mu}^+ c_{k,\mu} \rightarrow \sum_{\mu,n=0}^{\infty} [\epsilon_n f_{n,\mu}^+ f_{n,\mu} + \lambda_n (f_{n,\mu}^+ f_{n+1,\mu} + H.c.)] \quad (6)$$

with site energies, ϵ_n , and hoppings, λ_n , depending only on the dispersion ε_k and hybridization matrix elements V_{kd} through the hybridization function $\Delta(\omega)$ [9]. The Anderson model then takes the linear chain form

$$\begin{aligned} H_{AM} = & \varepsilon_d n_d + U n_{d\uparrow} n_{d\downarrow} + V \sum_{\mu} (f_{0,\mu}^+ d_\mu + d_\mu^+ f_{0,\mu}) \\ & + \sum_{\mu,n=0}^{\infty} [\epsilon_n f_{n,\mu}^+ f_{n,\mu} + \lambda_n (f_{n,\mu}^+ f_{n+1,\mu} + f_{n+1,\mu}^+ f_{n,\mu})] \end{aligned} \quad (7)$$

depicted in Fig. 3. Although, formally, this model looks like the one-dimensional real-space models treated by the DMRG method [10] in the lecture of Schollwöck, the interpretation here

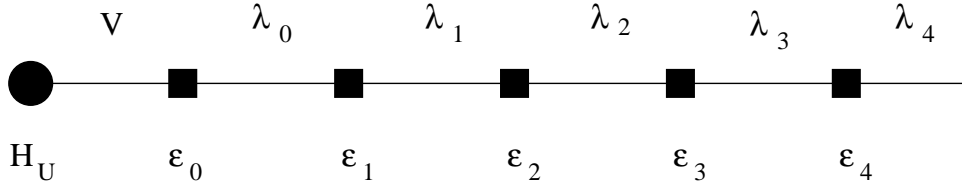


Fig. 3: The linear chain form of the Anderson model (7). $H_U = \varepsilon_d + U n_{d,\uparrow} n_{d,\downarrow}$. The “site energies” ε_n and “hoppings” λ_n follow from $\Delta(\omega)$.

is not in terms of electrons hopping on a one-dimensional lattice in real-space. Instead, as will become clearer in Sect. 3, each successive site added along the chain corresponds to adding lower energy degrees of freedom, measured relative to the Fermi level. By considering longer chains one can then access lower energies.

The same procedure can be used to reformulate any quantum impurity model in terms of an impurity site with local interactions attached to a one-dimensional chain of non-interacting sites. For example, the Kondo model (1) can be rewritten as

$$H_{KM} = J \vec{S} \cdot \vec{s}_0 + \sum_{\mu, n=0}^{\infty} [\varepsilon_n f_{n,\mu}^+ f_{n,\mu} + \lambda_n (f_{n,\mu}^+ f_{n+1,\mu} + f_{n+1,\mu}^+ f_{n,\mu})] \quad (8)$$

A zeroth order (high energy) approximation to the spectrum of the Anderson model can be obtained by considering just the coupling of the $n = 0$ Wannier state to the impurity and neglecting all others,

$$H_{AM} \approx H_0 = \varepsilon_d n_d + U n_{d\uparrow} n_{d\downarrow} + V \sum_{\mu} (f_{0,\mu}^+ d_{\mu} + d_{\mu}^+ f_{0,\mu}) \quad (9)$$

There are 16 many-electron states $|n_d, n_0\rangle$, which can be classified by the conserved quantum numbers of total electron number N_{el} , total z-component of spin S_z^{tot} and total spin \vec{S} . Using these symmetries we can diagonalize the block matrices H_{N_{el}, S, S_z}^0 to obtain the many-body eigenstates $|N_{el}, S, S_z, r\rangle$ and the corresponding eigenvalues. For example, in the product basis $|n_d\rangle|n_0\rangle$, the Hamiltonian for $N_e = 1, S = 1/2, S_z = \pm 1/2$ is given by

$$H_{N_e=1, S=1/2, S_z=\pm 1/2} = \begin{pmatrix} \varepsilon_d & V \\ V & 0 \end{pmatrix}$$

with eigenvalues

$$E_{\pm} = (\varepsilon_d \pm \sqrt{\varepsilon_d^2 + 4V^2})/2$$

Proceeding similarly for the other Hilbert spaces, we find that for the particle-hole symmetric case $\varepsilon_d = -U/2$ in the strong correlation limit $U \gg V^2$, the spectrum separates into two groups of states, one group of low energy states lying close to the (singlet) ground state with spacings $\mathcal{O}(V^2/U)$ and one group of high energy states lying at energies $\mathcal{O}(U/2)$ higher and also split by $\mathcal{O}(V^2/U)$. This limit corresponds to a singly occupied impurity level effectively behaving as a $S = 1/2$. In fact, the 8 lowest states correspond to those obtained from a zeroth order approximation to the spectrum of the Kondo model via

$$H_{KM} \approx H_0 = J \vec{S} \cdot \vec{s}_0 = \frac{J}{2} [(\vec{S} + \vec{s}_0)^2 - \vec{S}^2 - \vec{s}_0^2]. \quad (10)$$

The Kondo model is therefore the low energy effective model of the Anderson model in the limit of strong correlations and single occupancy. By comparing the splitting of the two lowest levels in the Kondo model, the singlet and triplet states, with the corresponding splitting of the same levels in the Anderson model one finds the relation between the bare parameters of the models (for the symmetric case) to be $J = 8V^2/U$. Slightly away from particle-hole symmetry, but still in the limit of large U , the relation becomes $J = 2V^2(\frac{1}{U+\varepsilon_d} - \frac{1}{\varepsilon_d})$, in agreement with that obtained from the Schrieffer-Wolff transformation [3].

Within the above zeroth order approximation of the Kondo model, excitations are unrenormalized. The singlet-triplet excitation takes the bare value J . The key ingredient of Wilson's NRG, to be discussed in the next section, is a controlled procedure for adding the remaining states $n = 1, 2, \dots$ neglected in the above approximation. As we shall see in the calculation of dynamical quantities below, this leads to a drastic renormalization of the spin and single-particle excitations, such that the relevant excitations of the Kondo model are not on the bare scale J but on the Kondo scale $T_K = D(\rho J)^{1/2} \exp(-1/\rho J)$, where $\rho = 1/2D$ is the density of conduction states (e.g., see Fig. 7-8 in Sect. 3). One can interpret this large renormalization $J \rightarrow T_K$ as a renormalization of a bare tunneling amplitude (J) due to the dissipative effects of the bath of conduction electrons.

3 Wilson's numerical approach

Wilson's formulation of the RG for the Kondo model is similar in spirit to Anderson's scaling method. The main difference lies in the non-perturbative construction of the RG transformation using a numerical representation of the effective Hamiltonians. The scaling approach uses perturbation theory in the initially small dimensionless coupling (J/D) to construct such a transformation, but since J/D increases with decreasing energy scale this approach eventually becomes inaccurate. In the Wilson approach the RG transformation is perturbative only via a small parameter $\Lambda^{-1/2} < 1$ which is related to the momentum rescaling factor $\Lambda > 1$. The accuracy of the transformation is the same at each step and is independent of the size of the running couplings. For this reason it gave the first correct description of the crossover from the weak coupling to the strong coupling regime of the Kondo model.

Separation of scales

In the Kondo problem, as in other quantum impurity problems, the behaviour of the system changes qualitatively over many energy scales as it passes through a crossover between fixed points (e.g. from behaviour characteristic of a well defined magnetic moment at high temperature to behaviour characteristic of a Fermi liquid at temperatures below the crossover scale). In order to describe this crossover the idea is to separate out the many energy scales in the problem, which arise from the conduction band $[-D, +D]$, and to set up a procedure for treating each scale in turn. We henceforth set $D = 1$ and assume a constant density of states $\rho(\varepsilon_k) = 1/2D$. A separation of energy scales is achieved by discretizing the conduction band into positive and negative energy intervals, $D_n^+ = [\Lambda^{-(n+1)}, \Lambda^{-n}]$ and $D_n^- = [-\Lambda^{-n}, -\Lambda^{-(n+1)}]$, $n = 0, 1, \dots$, about the Fermi level $\varepsilon_F = 0$ as shown in Fig. 4. By using $\sum_k F(k) = \int_{-1}^{+1} \rho(\varepsilon_k) d\varepsilon_k F(\varepsilon_k)$ and working in the energy representation $c_{k(\varepsilon), \mu} \rightarrow \rho(\varepsilon_k)^{-1/2} c_{\varepsilon, \mu}|_{\varepsilon=\varepsilon_k}$, we can carry out manipulations on the Kondo Hamiltonian (our derivations will be for a 1-dimensional dispersion ε_k , but

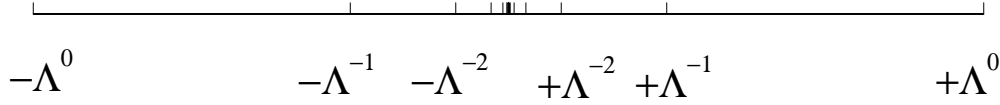


Fig. 4: Logarithmic discretization of the conduction band about the Fermi level $\epsilon_F = 0$

it can be generalized to a 3-dimensional dispersion $\epsilon_{\mathbf{k}}$: see Appendix A of [9]) to obtain,

$$\begin{aligned}
 H_{KM} &= \int_{-1}^{+1} d\varepsilon \varepsilon c_{\varepsilon,\mu}^+ c_{\varepsilon,\mu} + J\rho \underbrace{\int_{-1}^{+1} d\varepsilon \int_{-1}^{+1} d\varepsilon' c_{\varepsilon,\mu}^+ \vec{\sigma}_{\mu,\nu} c_{\varepsilon',\nu} \cdot \vec{S}}_{Jf_{0,\mu}^+ \vec{\sigma}_{\mu\nu} f_{0,\nu} \cdot \vec{S}}, \\
 &= \int_{-1}^{+1} d\varepsilon \varepsilon c_{\varepsilon,\mu}^+ c_{\varepsilon,\mu} + Jf_{0,\mu}^+ \vec{\sigma}_{\mu\nu} f_{0,\nu} \cdot \vec{S},
 \end{aligned} \tag{11}$$

where,

$$f_{0\mu} = \frac{1}{\sqrt{2}} \int_{-1}^{+1} d\varepsilon c_{\varepsilon,\mu} \tag{12}$$

is the Wannier state at the impurity.

Logarithmic discretization approximation

Most of the conduction electron states in (11) turn out to be irrelevant as far as impurity properties are concerned. One therefore uses the logarithmic discretization approximation to select just a subset of discrete states (which we justify below). Specifically, this approximation consists of choosing from each interval D_n^\pm just one state, the average electron state

$$c_{-n,\mu} \sim \int_{-\Lambda^{-n}}^{-\Lambda^{-(n+1)}} d\varepsilon c_{\varepsilon,\mu}$$

and the average hole state

$$c_{+n,\mu} \sim \int_{+\Lambda^{-(n+1)}}^{+\Lambda^{-n}} d\varepsilon c_{\varepsilon,\mu}$$

These states have energies

$$\varepsilon_{\pm n} = \pm \frac{1}{2} (\Lambda^{-n} + \Lambda^{-(n+1)}) = \pm \frac{1}{2} \Lambda^{-n} (1 + \Lambda^{-1}) \tag{13}$$

Of all the states one can construct in each interval D_{-n}^\pm , these are the states which are most localized near the impurity [9]. The infinite number of states $p = 1, 2, \dots$ neglected in each interval D_n^\pm are required to be orthogonal to the states defined above. This suggests that the states neglected $p = 1, 2, \dots$ will be centred at sites away from the impurity. A more precise argument shows that they are centred at distances $r \sim \Lambda^p$ from the impurity and that they only couple indirectly to the impurity (for the justification see Appendix B). Consequently they can

be neglected for the calculation of impurity properties. We therefore arrive at the discretized Kondo Hamiltonian

$$H \approx \sum_{n=0}^{\infty} (\varepsilon_{-n} c_{-n,\mu}^+ c_{-n,\mu} + \varepsilon_{+n} c_{+n,\mu}^+ c_{+n,\mu}) + J f_{0,\mu}^+ \vec{\sigma}_{\mu\nu} f_{0,\nu} \cdot \vec{S} \quad (14)$$

which as in (8) can be put into the linear chain form

$$H = \frac{1}{2} (1 + \Lambda^{-1}) \sum_{n=0}^{\infty} \Lambda^{-n/2} (f_{n,\mu}^+ f_{n,\mu} + f_{n+1,\mu}^+ f_{n,\mu}) + J f_{0,\mu}^+ \vec{\sigma}_{\mu\nu} f_{0,\nu} \cdot \vec{S}. \quad (15)$$

Here, we have used the explicit form of the Lanczos coefficients ϵ_n, λ_n appearing in (8) which were calculated analytically in [1] for a logarithmically discretized conduction band: $\epsilon_n = 0$ and $\lambda_n \approx \frac{1}{2} (1 + \Lambda^{-1}) \Lambda^{-n/2}, n \gg 1$. This form of the Hamiltonian provides a clear separation of the energy scales $\frac{1}{2} (1 + \Lambda^{-1}) \Lambda^{-n/2}, n = 1, 2, \dots$ in H and allows the diagonalization of the Hamiltonian in a sequence of controlled steps, each step corresponding to adding an orbital $f_{n,\mu}$ which is a relative perturbation of strength $\Lambda^{-1/2} < 1$. Although, formally, we could obtain in (8) the linear chain form of the Kondo model without using the logarithmic discretization approximation, in practice, the decay of the coefficients λ_n , and hence the convergence of the method, is only guaranteed for such a discretization.

RG transformation

A RG transformation relating effective Hamiltonians on successive energy scales $\Lambda^{-n/2}$ and $\Lambda^{-(n+1)/2}$ can be set up as follows. First, H in (15) is truncated to N orbitals to give H_N , whose lowest scale is $D_N = \frac{1}{2} (1 + \Lambda^{-1}) \Lambda^{-(N-1)/2}$. In order to look for fixed points we define rescaled Hamiltonians $\bar{H}_N \equiv H_N / D_N$ such that the lowest energy scale of \bar{H}_N is always of $\mathcal{O}(1)$:

$$\bar{H}_N = \Lambda^{(N-1)/2} \left[\sum_{n=0}^{N-1} \Lambda^{-n/2} (f_{n,\mu}^+ f_{n,\mu} + f_{n+1,\mu}^+ f_{n,\mu}) + \tilde{J} f_{0,\mu}^+ \vec{\sigma}_{\mu\nu} f_{0,\nu} \cdot \vec{S} \right], \quad (16)$$

$$\tilde{J} = \frac{2J\rho}{\frac{1}{2}(1 + \Lambda^{-1})}, \quad (17)$$

from which we can recover H as

$$H = \lim_{N \rightarrow \infty} \frac{1}{2} (1 + \Lambda^{-1}) \Lambda^{-(N-1)/2} \bar{H}_N. \quad (18)$$

The sequence of rescaled Hamiltonians \bar{H}_N satisfies the recursion relation

$$\bar{H}_{N+1} = \Lambda^{1/2} \bar{H}_N + (f_{N,\mu}^+ f_{N+1,\mu} + f_{N+1,\mu}^+ f_{N,\mu}), \quad (19)$$

and allows a RG transformation \mathcal{T} to be defined:

$$\bar{H}_{N+1} = \mathcal{T}[\bar{H}_N] \equiv \Lambda^{1/2} \bar{H}_N + (f_{N,\mu}^+ f_{N+1,\mu} + f_{N+1,\mu}^+ f_{N,\mu}) - \bar{E}_{G,N+1} \quad (20)$$

with $\bar{E}_{G,N+1}$ the ground state energy of \bar{H}_{N+1} . In fact \mathcal{T} defined in (20) does not have fixed points since it relates a Hamiltonian \bar{H}_{2n} with an odd number of orbitals $N = 0, 1, \dots, 2n$ to a Hamiltonian \bar{H}_{2n+1} with an even number of orbitals $N = 0, 1, \dots, 2n+1$ or vice versa. The even/odd spectra do not match for the Kondo model. However, $\mathcal{R} = \mathcal{T}^2$, can be defined as the RG transformation and this will have fixed points, a set of even N fixed points and a set of odd N fixed points:

$$\bar{H}_{N+2} = \mathcal{R}[\bar{H}_N] \equiv \mathcal{T}^2[\bar{H}_N] \quad (21)$$

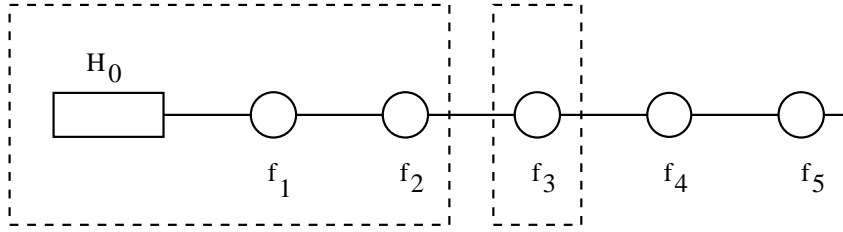


Fig. 5: Iterative diagonalization scheme for H , starting with H_0 and then adding successive orbitals f_1, f_2, \dots

Iterative diagonalization scheme

The transformation R relates effective Hamiltonians $H_N = D_N \bar{H}_N$ and $H_{N+1} = D_{N+1} \bar{H}_{N+1}$ on decreasing scales $D_N > D_{N+1}$. It can be used to iteratively diagonalize the Kondo Hamiltonian by the following sequence of steps:

1. the local part

$$\bar{H}_0 = \Lambda^{-1/2} \tilde{J} f_{0,\mu}^+ \vec{\sigma}_{\mu\nu} f_{0,\nu} \cdot \vec{S} = \Lambda^{-1/2} \tilde{J} \vec{s}_0 \cdot \vec{S}, \quad (22)$$

which contains the many-body interactions, is diagonalized (the “zeroth” order step described in Sect. 2),

2. assuming that \bar{H}_N has been diagonalized,

$$\bar{H}_N = \sum_{\lambda} \bar{E}_{\lambda}^N |\lambda\rangle \langle \lambda| \quad (23)$$

we add a “site” and use (20) to set up the matrix for \bar{H}_{N+1} within a product basis

$$|\lambda, i\rangle = |\lambda\rangle_N |i\rangle_{N+1} \quad (24)$$

consisting of the eigenstates $|\lambda\rangle_N$ of \bar{H}_N and the 4 states $|i\rangle_{N+1}$ of the next orbital along the chain (i.e. $|i\rangle_{N+1} = |0\rangle, |\uparrow\rangle, |\downarrow\rangle, |\uparrow\downarrow\rangle$). The resulting matrix

$$\begin{aligned} \langle \lambda, i | \bar{H}_{N+1} | \lambda', i' \rangle &= \Lambda^{1/2} \delta_{i,i'} \delta_{\lambda,\lambda'} \bar{E}_{\lambda}^N \\ &+ (-1)^{N_{e,\lambda'}} \langle \lambda | f_{N,\mu}^+ | \lambda' \rangle \langle i | f_{N+1,\mu} | i' \rangle \\ &+ (-1)^{N_{e,\lambda}} \langle i | f_{N+1,\mu}^+ | i' \rangle \langle \lambda | f_{N,\mu} | \lambda' \rangle, \end{aligned}$$

with $N_{e,\lambda}, N_{e,\lambda'}$ the number of electrons in $|\lambda\rangle, |\lambda'\rangle$ respectively, is diagonalized and the procedure is repeated for the next energy shell as depicted in Fig. 5. Since \bar{H}_N is already diagonalized, the off-diagonal matrix elements, involving ${}_N \langle \lambda | f_{N,\mu} | \lambda' \rangle_N$, can be expressed in terms of the known eigenstates of \bar{H}_N (see [9] for explicit expressions).

Truncation

In practice since the number of many-body states in \bar{H}_N grows as 4^N it is not possible to retain all states after about $N = 5$. For $N > 5$ only the lowest 1000 or so states of \bar{H}_N are retained. The truncation of the spectrum of \bar{H}_N restricts the range of eigenvalues in $H_N = D_N \bar{H}_N$ to be such that $0 \leq E_{\lambda}^N \leq K D_N$ where $K = K(\Lambda)$ depends on Λ and the number of states

retained. For 1000 states and $\Lambda = 3$, $K(\Lambda) \approx 10$. However, eigenvalues below D_N are only approximate eigenvalues of the infinite system H , since states with energies below D_N are calculated more accurately in subsequent iterations $N+1, N+2, \dots$. Therefore the part of the spectrum of H_N which is close to the spectrum of H is restricted to $D_N \leq E_\lambda^N \leq K(\Lambda)D_N$. This allows the whole spectrum of H to be recovered by considering the spectra of the sequence of Hamiltonians H_N , $N = 0, 1, \dots$. In this way the many-body eigenvalues and eigenstates are obtained on all energy scales. Due to the smallness of the perturbation (of $\mathcal{O}(\Lambda^{-1/2}) < 1$) in adding an energy shell to go from H_N to H_{N+1} , the truncation of the high energy states turns out, in practice, to be a very good approximation.

Comparison with real space RG methods

Real space RG methods have been used very successfully to investigate second order phase transitions [11]. In these methods, the form of the effective Hamiltonians, H_N , is such that only a small number of couplings (e.g. nearest-neighbour and next-nearest-neighbour couplings in the case of the 2D Ising model) is retained during the RG procedure. Despite this, highly accurate results can be obtained for critical properties. The reason for this is that second order critical points are governed by just a few relevant couplings, so an effective Hamiltonian retaining just these couplings is sufficient to describe the critical behaviour. In contrast, for the Kondo model, and, for quantum impurity models in general, the interest is in obtaining information about the many-body eigenstates and eigenvalues on all energy scales and not just close to a particular fixed point where simplifying assumptions about the effective Hamiltonian might hold. Consequently, a general form of the effective Hamiltonians, including relevant and irrelevant couplings, is required in order to follow the behaviour of the system as it flows via various unstable fixed points to the stable fixed point describing the interacting quantum mechanical groundstate. Such a general form is possible in the Kondo calculation as a result of the numerical representation of the H_N .

Comparison with DMRG

The DMRG method, described in the lecture Schollwöck, differs from the NRG approach used in the Kondo calculation in several ways. The most important, and the reason for its success as applied to one-dimensional lattice models, is the criterion for choosing the basis states of the subsystems (the “block”, H_N in the Kondo calculation) used to extend the size of the system (the “superblock”, H_{N+1} in the Kondo calculation). These are chosen according to their weight in a reduced density matrix built from a few eigenstates of the larger system (in the Kondo calculation this reduced density matrix would be $\rho_N^{red} = \sum_i \langle i | \rho_{N+1} | i \rangle$ where $|i\rangle$ are the states of the $N+1$ 'th site and ρ_{N+1} is the density matrix of H_{N+1}). That is, the states retained in the subsystems (similar to the lowest states retained in \bar{H}_N in the Kondo calculation) are in this case not necessarily the lowest energy states, but they are the states which couple most strongly, in the sense of having large eigenvalues in the reduced density matrix describing the subsystem, to the ones of interest, the target states of the larger system (in the Kondo calculation these might be taken to be the lowest few eigenstates of \bar{H}_{N+1}). The procedure gives highly accurate results for these target states, and therefore improves on real space NRG methods.

4 Calculation of physical properties

Applications of the NRG to quantum impurity models fall into three areas: analysis of fixed points, calculation of thermodynamics and calculation of dynamic and transport properties.

The analysis of fixed points is important to gain a conceptual understanding of the model and for accurate analytic calculations in the vicinity of a fixed point (e.g. near the groundstate). The ability of the method to yield thermodynamic, dynamic and transport properties makes it very useful for interpreting experimental results.

Fixed Points

From (21), a fixed point H^* of $\mathcal{R} = \mathcal{T}^2$ is defined by

$$H^* = \mathcal{R}[H^*]. \quad (25)$$

Proximity to a fixed point is identified by ranges of N , $N_1 \leq N \leq N_2$, where the energy levels \bar{E}_p^N of \bar{H}_N are approximately independent of N : $\bar{E}_p^N \approx \bar{E}_p$ for $N_1 \leq N \leq N_2$. A typical energy level flow diagram showing regions of N where the energy levels are approximately constant is shown in Fig. 6 for the anisotropic Kondo model (AKM) [12]:

$$H_{AKM} = \sum_{k\mu} \varepsilon_k c_{k\mu}^\dagger c_{k\mu} + \frac{J_\perp}{2} (S^+ f_{0\downarrow}^\dagger f_{0\uparrow} + S^- f_{0\uparrow}^\dagger f_{0\downarrow}) + \frac{J_\parallel}{2} S_z (f_{0\uparrow}^\dagger f_{0\uparrow} - f_{0\downarrow}^\dagger f_{0\downarrow}) \quad (26)$$

There is an unstable high energy fixed point (small N) and a stable low energy fixed point (large N). The low energy spectrum is identical to that of the isotropic Kondo model at the strong coupling fixed point $J = \infty$ in [1] (e.g. the lowest single particle excitations in Fig. 6, $\eta_1 = 0.6555$, $\eta_2 = 1.976$ agree with the $\Lambda = 2$ results of the isotropic model in [1]). The crossover from the high energy to the low energy fixed point is associated with the Kondo scale T_K . Spin-rotational invariance, broken at high energies, is restored below this scale (e.g. the $j = 0$ states with $S_z = 0$ and $S_z = \pm 1$ become degenerate below T_K and can be classified by the same total spin S as indicated in Fig. 6). Analytic calculations can be carried out in the vicinity of fixed points by setting up effective Hamiltonians $H_{eff} = H^* + \sum_\lambda \omega_\lambda O_\lambda$, where the leading deviations O_λ about H^* can be obtained from general symmetry arguments. This allows, for example, thermodynamic properties to be calculated in a restricted range of temperatures, corresponding to the restricted range of N where \bar{H}_N can be described by a simple effective Hamiltonian H_{eff} . In this way Wilson could show that the ratio of the impurity susceptibility, χ_{imp} , and the impurity contribution to the linear coefficient of specific heat, γ_{imp} , at $T = 0$, is twice the value of a non-interacting Fermi liquid: $R = \frac{4\pi^2 \chi_{imp}}{3\gamma_{imp}} = 2$. We refer the reader to the detailed description of such calculations in [1,9], and we turn now to the numerical procedure for calculating thermodynamics, which can give results at all temperatures, including the crossover regions.

Thermodynamics

Suppose we have diagonalized exactly the Hamiltonian for a quantum impurity model such as the Kondo model and that we have all the many-body eigenvalues E_λ and eigenstates $|\lambda\rangle$:

$$H = \sum_\lambda E_\lambda |\lambda\rangle \langle \lambda| \equiv \sum_\lambda E_\lambda X_{\lambda\lambda}. \quad (27)$$

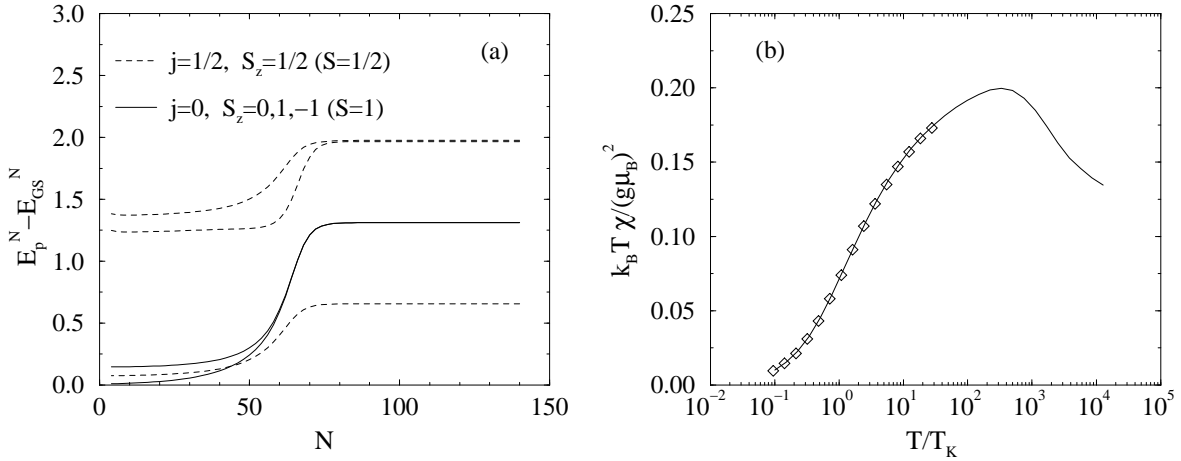


Fig. 6: (a) The lowest rescaled energy levels of the AKM for $J_{\parallel} = 0.443$ and $J_{\perp} = 0.01$. The states are labeled by conserved pseudospin j and total S_z [12]. In (b) the static susceptibility of the Anderson impurity model for $U/\pi\Delta = 6$, $\varepsilon_d/\Delta = -5$ (full curve) is shown. The symbols are from the universal susceptibility curve for the isotropic Kondo model (taken from Table V of [9]), which agrees with the low temperature susceptibility of the Anderson model.

We can then calculate the partition function

$$Z(T) \equiv \text{Tr} e^{-H/k_B T} = \sum_{\lambda} e^{-E_{\lambda}/k_B T}, \quad (28)$$

and hence the thermodynamics via the impurity contribution to the free energy $F_{\text{imp}}(T) = -k_B T \ln Z/Z_c$, where $Z_c = \text{Tr} e^{-H_c/k_B T}$ is the partition function for the non-interacting conduction electrons. In the NRG procedure we can only calculate the "partition functions" Z_N for the sequence of truncated Hamiltonians H_N :

$$Z_N(T) \equiv \text{Tr} e^{-H_N/k_B T} = \sum_{\lambda} e^{-E_{\lambda}^N/k_B T} = \sum_{\lambda} e^{-D_N \bar{E}_{\lambda}^N/k_B T} \quad (29)$$

We will have $Z_N(T) \approx Z(T)$ provided

1. we choose $k_B T = k_B T_N \ll E_{\text{max}}^N = D_N K(\Lambda)$ so that the contribution to the partition function from excited states $E_{\lambda}^N > D_N K(\Lambda)$, not contained in Z_N , is negligible, and
2. the truncation error made in replacing H by H_N in equating (28) and (29) is small. This error has been estimated in [9] to be approximately $\Lambda^{-1} D_N / k_B T_N$.

Combining these two conditions requires that

$$\frac{1}{\Lambda} \ll \frac{k_B T_N}{D_N} \ll K(\Lambda). \quad (30)$$

The choice $k_B T = k_B T_N \approx D_N$ is reasonable and allows the thermodynamics to be calculated at a sequence of decreasing temperatures $k_B T_N \sim D_N$, $N = 0, 1, \dots$ from the truncated partition functions Z_N . The procedure is illustrated in Fig. 6 for the impurity static susceptibility of the Anderson impurity model

$$\chi_{\text{imp}}(T) = \frac{(g\mu_B)^2}{k_B T} \left[\frac{1}{Z} \text{Tr} (S_z^{\text{tot}})^2 e^{-H/k_B T} - \frac{1}{Z_c} \text{Tr} (S_{z,c}^{\text{tot}})^2 e^{-H_c/k_B T} \right].$$

Dynamic properties

We consider now the application of the NRG method to the calculation of dynamic properties of quantum impurity models [13, 14]. For definiteness we consider the Anderson impurity model and illustrate the procedure for the impurity spectral density $\rho_{d,\mu}(\omega, T) = -\frac{1}{\pi} \text{Im} G_{d,\mu}(\omega, T)$, with

$$G_{d,\mu}(\omega, T) = \int_{-\infty}^{+\infty} d(t-t') e^{i\omega(t-t')} G_{d,\mu}(t-t') \quad (31)$$

$$G_{d,\mu}(t-t') = -i\theta(t-t') \langle [d_\mu(t), d_\mu^\dagger(t')]_+ \rangle_\varrho \quad (32)$$

with ϱ the density matrix of the system.

Suppose we have all the many-body eigenstates $|\lambda\rangle$ and eigenvalues E_λ of the Anderson impurity Hamiltonian H . Then the density matrix, $\varrho(T)$, of the full system at temperature $k_B T = 1/\beta$ can be written

$$\varrho(T) = \frac{1}{Z(T)} \sum_{\lambda} e^{-\beta E_\lambda} |\lambda\rangle \langle \lambda|, \quad (33)$$

and the impurity Green's function can be written in the Lehmann representation as

$$G_{d,\mu}(\omega, T) = \frac{1}{Z(T)} \sum_{\lambda, \lambda'} |\langle \lambda | d_\mu | \lambda' \rangle|^2 \frac{e^{-E_\lambda/k_B T} + e^{-E_{\lambda'}/k_B T}}{\omega - (E_{\lambda'} - E_\lambda)} \quad (34)$$

and the corresponding impurity spectral density $\rho_{d,\mu}$ as

$$\rho_{d,\mu}(\omega, T) = \frac{1}{Z(T)} \sum_{\lambda, \lambda'} |M_{\lambda, \lambda'}|^2 (e^{-E_\lambda/k_B T} + e^{-E_{\lambda'}/k_B T}) \delta(\omega - (E_{\lambda'} - E_\lambda)) \quad (35)$$

with $M_{\lambda, \lambda'} = \langle \lambda | d_\mu | \lambda' \rangle$.

Consider first the $T = 0$ case ($T > 0$ is described in the next section), then

$$\rho_{d,\mu}(\omega, T = 0) = \frac{1}{Z(0)} \sum_{\lambda} |M_{\lambda, 0}|^2 \delta(\omega + (E_\lambda - E_0)) + \frac{1}{Z(0)} \sum_{\lambda'} |M_{0, \lambda'}|^2 \delta(\omega - (E_{\lambda'} - E_0)), \quad (36)$$

with $E_0 = 0$ the ground state energy. In order to evaluate this from the information which we actually obtain from an iterative diagonalization of H , we consider the impurity spectral densities corresponding to the sequence of Hamiltonians H_N , $N = 0, 1, \dots$,

$$\rho_{d,\mu}^N(\omega, T = 0) = \frac{1}{Z_N(0)} \sum_{\lambda} |M_{\lambda, 0}^N|^2 \delta(\omega + E_\lambda^N) + \frac{1}{Z_N(0)} \sum_{\lambda'} |M_{0, \lambda'}^N|^2 \delta(\omega - E_{\lambda'}^N). \quad (37)$$

From the discussion on the spectrum of H_N in the previous section, it follows that the ground-state excitations of H_N which are representative of the infinite system H are those in the range $D_N \leq \omega \leq K(\Lambda)D_N$. Lower energy excitations and eigenstates are calculated more accurately at subsequent iterations, and higher energy excitations are not contained in H_N due to the elimination of the higher energy states at each N . Hence, for fixed N , and provided that the matrix elements $M_{0, \lambda'}^N$ are also approximately those of the infinite system $M_{0, \lambda}$ we have

$$\rho_{d,\mu}^N(\omega, T = 0) \approx \rho_{d,\mu}(\omega, T = 0) \quad (38)$$

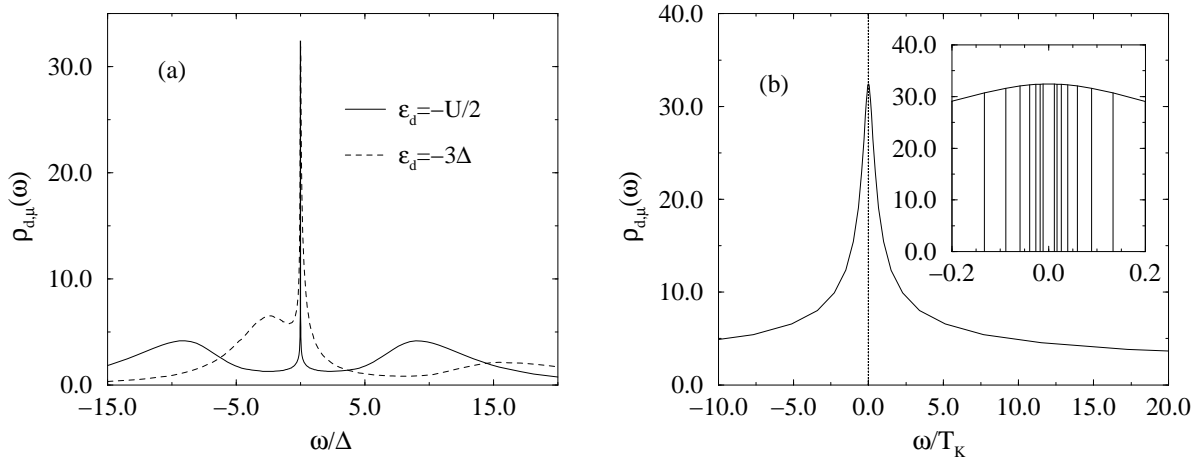


Fig. 7: (a) The impurity spectral density for the Anderson impurity model for $U/\pi\Delta = 6$ and different local level positions. The Kondo resonance for the case $\varepsilon_d = -U/2$ is shown in more detail in (b). The vertical lines in the inset show the sequence of energies $\omega = 2\omega_N$ at which the spectral density is calculated and demonstrates the ability of the method to resolve low energy scales.

provided that we choose $\omega \approx \omega_N \equiv k_B T_N$ to lie in the range described by H_N . A typical choice is $\omega = 2\omega_N$ for $\Lambda = 2$. This allows $\rho_{d,\mu}(\omega, T = 0)$ to be calculated at a sequence of decreasing frequencies $\omega = 2\omega_N, N = 0, 1, \dots$ from the quantities $\rho_{d,\mu}^N$. In practice we are not interested in the discrete spectra $\rho_{d,\mu}^N(\omega) = \sum_{\lambda} w_{\lambda}^N \delta(\omega - E_{\lambda}^N)$ of the Hamiltonians H_N but in continuous spectra which can be compared with experiment. Smooth spectra can be obtained from the discrete spectra by replacing the delta functions $\delta(\omega - E_{\lambda}^N)$ by smooth distributions $P_N(\omega - E_{\lambda}^N)$. A natural choice for the width η_N of P_N is D_N , the characteristic scale for the energy level structure of H_N . Two commonly used choices for P are the Gaussian and the Logarithmic Gaussian distributions [13–15]. A peak of intrinsic width Γ at frequency Ω_0 will be well resolved by the above procedure provided that $\Omega_0 \ll \Gamma$, which is the case for the Kondo resonance and other low energy resonances. In the opposite case, the low (logarithmic) resolution at higher frequencies may be insufficient to resolve the intrinsic widths and heights of such peaks. Usually such higher frequency peaks are due to single-particle processes and can be adequately described by other methods (exceptions include interaction dominated features in the Ohmic two-state system, see below, and in strongly correlated lattice models in high dimensions [16]). In both cases, $\Omega_0 \ll \Gamma$ and $\Omega_0 \gg \Gamma$, the positions and intensities of such peaks is given correctly. An alternative procedure for obtaining smooth spectra, which in principle resolves finite frequency peaks with the same resolution as the low energy peaks, has been proposed in [17]. This involves a modified discretization of the conduction band with energies $\pm 1, \pm \Lambda^{-z}, \pm \Lambda^{-z-1}, \dots$ instead of the usual discretization $\pm 1, \pm \Lambda^{-1}, \pm \Lambda^{-2}, \dots$. By considering all z between 0 and 1 one recovers a continuous spectrum without the need to use a broadening function. The procedure requires diagonalizing H for many values of z . It has also proved useful for carrying out thermodynamic calculations at large Λ [18].

How accurate is the NRG for dynamic properties? In Fig. 7 we show results for $T = 0$ spectral densities of the Anderson impurity model [14]. A good measure of the accuracy of the

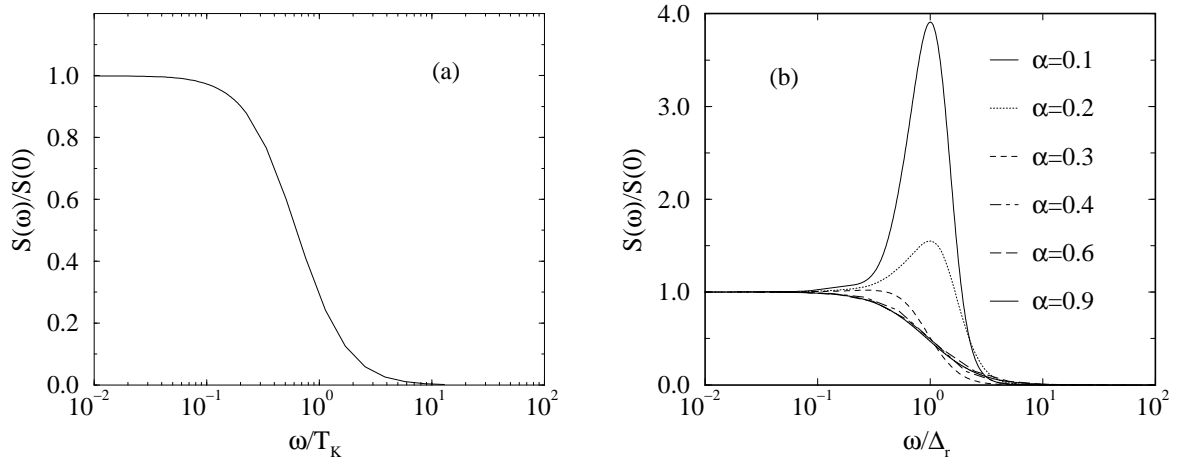


Fig. 8: The $T = 0$ longitudinal spin-relaxation function, $S(\omega)$, for **(a)** the Anderson impurity model for $U/\pi\Delta = 6$ and $\varepsilon_d = -5\Delta$, and **(b)** the AKM for increasing values of the coupling ρJ_{\parallel} corresponding to decreasing values of the dissipation strength α in the equivalent Ohmic two-state system [12] ($\Delta_r = T_K$).

procedure is given by the Friedel sum rule, a Fermi liquid relation which states that [3]

$$\rho_{d,\mu}(0) = \frac{1}{\pi\Delta} \sin^2(\pi n_d/2), \quad n_d = \int_{-\infty}^0 d\omega \rho_{d,\mu}(\omega) \quad (39)$$

The integrated value of n_d , for the spectral density shown in Fig. 7, is 0.991. Including the renormalization in Δ due to the discretization, as discussed in [9], gives $\rho_{d,\mu}(0) = 32.779$. The value extracted directly from Fig. 7 is $\rho_{d,\mu}(0) = 32.31$ resulting in a 1.4% error, most of which is due to using the integrated value of n_d over all energy scales. Calculating n_d solely from the low energy part of the spectrum (e.g. as the limit $n_d(T \rightarrow 0)$ in a thermodynamic calculation) further reduces this error. More important, however, is that the error remains small independent of the interaction strength $0 \leq U \leq \infty$.

Two-particle Green functions and response functions can also be calculated. Fig. 8 shows the longitudinal spin relaxation function

$$S(\omega) = -\frac{1}{\pi} \frac{\text{Im}\chi_{zz}(\omega)}{\omega}, \quad \chi_{zz} = \langle\langle S_z; S_z \rangle\rangle$$

of the Anderson impurity model and of the AKM [12]. The former always exhibits incoherent spin dynamics. It is interesting that the latter can exhibit coherent spin dynamics for sufficiently large ρJ_{\parallel} .

Transport properties

The transport properties of quantum impurity models, require knowledge of both the frequency and temperature dependence of the impurity spectral density. The resistivity $\rho(T)$ of conduction electrons scattering from a single Anderson impurity, for example, is given by the expression

$$\rho(T)^{-1} = -e^2 \int_{-\infty}^{+\infty} \tau_{tr}(\omega, T) \frac{\partial f}{\partial \omega} d\omega \quad (40)$$

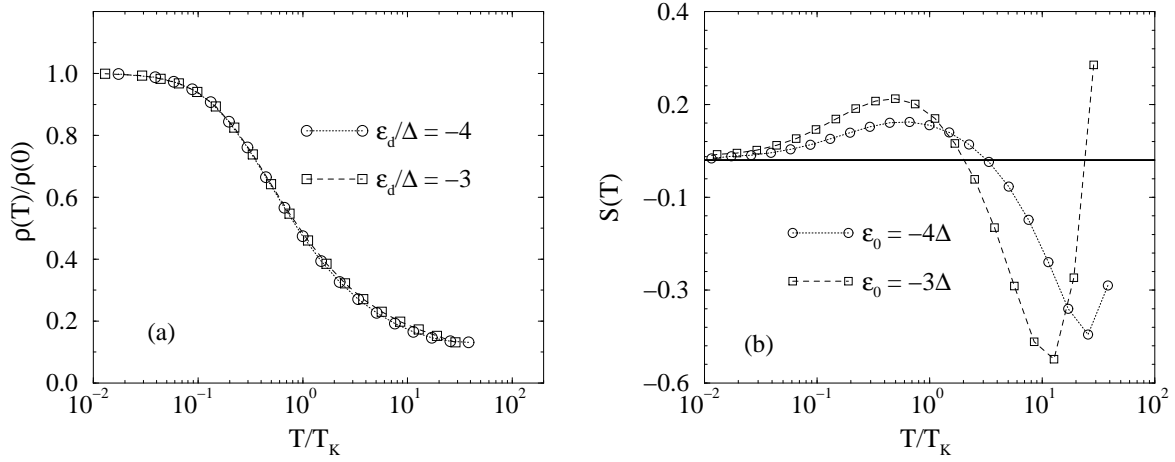


Fig. 9: (a) The scaled resistivity $\rho(T)/\rho(0)$ and (b) the thermopower $S(T)$ of the Anderson impurity model for $U/\pi\Delta = 4$ and two values of the local level position in the Kondo regime [14].

where the transport time $\tau_{tr}(\omega, T)$ is related to the impurity spectral density by $\tau_{tr}^{-1}(\omega, T) = \Delta \rho_{d,\mu}(\omega, T)$ and Δ is the hybridization strength. Similar expressions hold for the other transport coefficients.

The procedure for calculating finite temperature dynamical quantities, like $\rho_{d,\mu}(\omega, T)$, required as input for calculating transport properties, is similar to that for $T = 0$ dynamics described above [14]. The spectral density $\rho_{d,\mu}(\omega, T)$ at fixed temperature T is evaluated as above at frequencies $\omega \approx 2\omega_N$, $N = 0, 1, \dots, M$ until $2\omega_M$ becomes of order $k_B T$. To calculate the spectral density at frequencies $\omega < k_B T$ a smaller “cluster” is used. This is done because when $k_B T$ is larger than the frequency at which the spectral density is being evaluated, it is the excited states of order $k_B T$ contained in previous clusters that are important and not the excitations very much below $k_B T$.

Results for the resistivity and thermopower of the Anderson impurity model are shown in Fig. 9. The method gives uniformly accurate results at high and low temperatures, as well as correctly describing the crossover region $T \approx T_K$ (detailed comparisons of the resistivity with known results at high and low temperature can be found [14]). These resistivity calculations, and similar conductance calculations for quantum dots [19], provide a quantitative interpretation of experiments for $S = 1/2$ realizations of the Kondo effect .

5 Recent developments

The reduced density matrix and NRG

In evaluating the $T = 0$ dynamics in Sect. 4 the approximation (38) was made that the excitations E_λ^N and matrix elements $M_{0,\lambda}^N$ of the N ’th “cluster Hamiltonian”, H_N , were close to those of the infinite system. This is certainly correct for large N , and explicit calculation demonstrates that the approximation is close to exact for most cases. However, this approximation to the dynamics fails in certain cases. For example, when an applied field strongly perturbs the ground state and low lying excited states, as happens for the Anderson model in a magnetic

field [20]. In this case the overlap matrix elements $M_{0,\lambda}^N = \langle 0 | d_\mu | \lambda \rangle$ connecting the ground state and excited states of H_N may deviate significantly from those of the infinite system. This will mainly affect the spectra for small N , i.e. at high energies. In order to overcome this problem [20] one can make use of the reduced density matrix, ϱ_N^{red} , of H_N , obtained from the density matrix, $\varrho_M(T=0)$, of a much larger cluster, $H_{M \gg N}$, whose ground state is closer to that of the infinite system, by tracing out intermediate degrees of freedom

$$\varrho_N^{red} = \text{Tr}_{i_{N+1}, \dots, i_M} \varrho_M \quad (41)$$

Using ϱ_N^{red} in place of ϱ in (32) results in the Lehmann representation for the spectral density

$$\rho_{d,\mu}(\omega, T=0) = \sum_{\kappa, \lambda} C_{\kappa, \lambda} M_{\kappa, \lambda}^N \delta(\omega - (E_\kappa^N - E_\lambda^N)) \quad (42)$$

$$C_{\kappa, \lambda} = \sum_{\nu} \rho_{\nu, \lambda}^{red} M_{\nu, \kappa}^N + \sum_{\nu} \rho_{\kappa, \nu}^{red} M_{\lambda, \nu}^N \quad (43)$$

in place of (36). This is evaluated, as in (38), at $\omega \approx 2\omega_N$. Note that the use of the reduced density matrix “feeds back” information about the ground state of the larger clusters into the smaller clusters, but the excitation energies of cluster N , $E_\kappa^N - E_\lambda^N$, which are only approximately equal to those of the infinite system, are not corrected for by using the reduced density matrix. Fig. 10 shows corrections to Kondo model spectra in a finite magnetic field using the reduced density matrix.

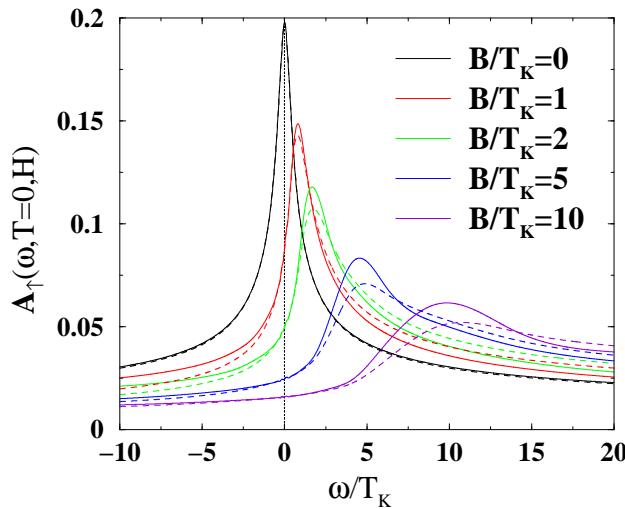


Fig. 10: Comparison of spectra for the Kondo model in a magnetic field [19] with (dashed lines) and without (solid lines) the use of the reduced density matrix. The reduced density matrix provides much more significant corrections for the high energy features in the spin-resolved spectra of the Anderson model, as shown in [20]

Non-equilibrium quantities in NRG

The application of a finite transport voltage across a semiconducting quantum dot [21] (see Fig. 11) modelled by an Anderson impurity model creates a non-equilibrium state which for sufficiently large transport voltage can not be described within linear response theory. One would like to understand both the transient dynamics of the system after the initial switching on of the field, and also the steady state dynamics in the long time limit. An approach to transient response within NRG has recently been developed [22, 23] in analogy to the X-ray problem of core-level spectroscopy [24]. To illustrate this, consider the time-dependent dynamics of a

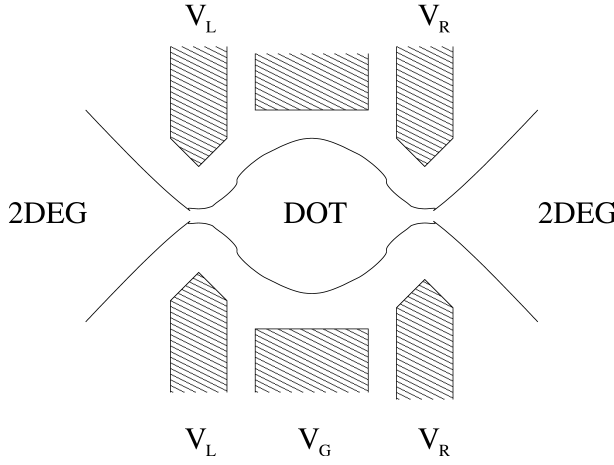


Fig. 11: Top view of a quantum dot. A confined region of electrons (the “quantum dot”) is formed out of the two dimensional electron gas (2DEG) at the interface of a GaAs/AlGaAs heterostructure by patterning electrodes as shown and applying negative voltages. The constrictions at the left and right connect the dot electrons to the remaining 2DEG. Confinement implies district levels and large Coulomb repulsion on the dot, so this system behaves like an Anderson impurity model with tunable hybridization matrix elements (via $V_{L,R}$) and level position (via V_G).

Kondo spin subject to an initial state preparation at $t < 0$ and a sudden perturbation at $t = 0$ of the form

$$H(t) = [1 - \theta(t)]H_I + \theta(t)H_F \quad (44)$$

We take the initial state Hamiltonian, H_I , to be the anisotropic Kondo model with a local magnetic field $-BS_z$, $B \rightarrow \infty$ forcing the spin to have $\langle S_z \rangle = 1/2$ for times $t < 0$ and the final state Hamiltonian, H_F , to be H_{AKM} with the local magnetic field switched off. An interesting question is whether $P(t) = \langle S_z(t) \rangle_{\varrho_I}$, with $\varrho_I = e^{-\beta H_I}$, exhibits coherent or incoherent dynamics. By obtaining the many-body eigenstates $|m_I\rangle$ ($|m_F\rangle$) and eigenvalues E_{m_I} (E_{m_F}) of H_I (H_F) using the NRG, one can obtain the Fourier transform of $P(t)$ in Lehmann representation

$$P(\omega) = \sum_{m_I, m_F, m'_F} \frac{e^{-\beta E_{m_I}}}{Z_I} \langle m_I | m_F \rangle \langle m'_F | m_I \rangle \langle m_F | S_z | m'_F \rangle \delta(\omega - (E_{m_F} - E_{m'_F})) \quad (45)$$

In contrast to equilibrium dynamical quantities (36), no ground state energy appears in the above expression for $P(\omega)$ (even for $T = 0$), reflecting the absence of a ground state in a non-equilibrium situation. This also implies, that in evaluating (45), at a frequency $\omega = \omega_N$ we cannot simply use the excitations of H_F from a single cluster $M = N$. Instead excitations between arbitrary excited states of H_F arising from all cluster sizes contribute and have to be taken into account [22]. The approximation of using a single shell $M = N$ to evaluate (45) at $\omega = \omega_N$,

$$P(\omega_N) \approx \sum_{m_F, m'_F} \langle m_{I,GS} | m_F \rangle_N \langle m'_F | m_{I,GS} \rangle_N \langle m_F | S_z | m'_F \rangle_N \delta(\omega - (E_{m_F}^N - E_{m'_F}^N)) \quad (46)$$

is valid for short time scales ($t \leq 1/T_K$) or high frequencies ($\omega \gg T_K$). Typical results are shown in Fig. 12. Recently, the problem of summing over all energy shells proposed in [22] has been solved [23]. In [23], a complete basis set of states for the Hilbert space of $H_{I,F}$ is used, made up not from the retained states of the $H_{I,F}^N$, but from the high energy states eliminated at each step N . Since, as $N \rightarrow \infty$, all states are eliminated, the set of all eliminated states is a complete eigenbasis of $H_{I,F}$. This allows contributions to $P(\omega)$ from all energy shells to be summed up, thereby allowing the study of the long-time behaviour of transient dynamics [23].

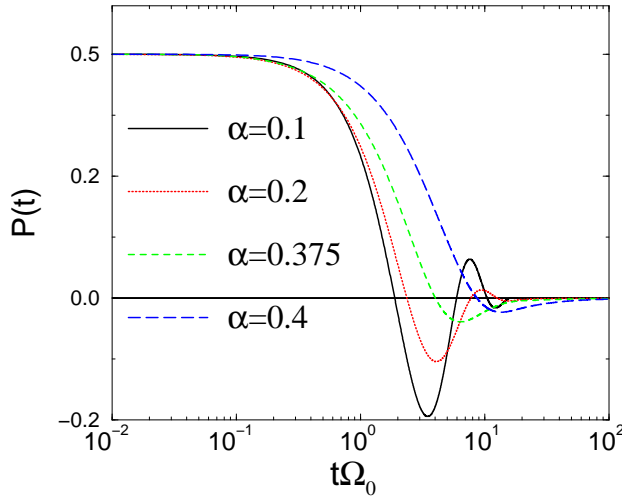


Fig. 12: $P(t) = \langle S_z(t) \rangle$ for the AKM obtained from Fourier transforming the $P(\omega)$ [22] of (46) for several ρJ_{\parallel} corresponding to the dissipation strengths $\alpha = (1 - \frac{2}{\pi} \tan^{-1}(\pi \rho J_{\parallel}/4))^2$ shown in the figure. The crossover to incoherent behaviour occurs at $\alpha = 1/2$. Ω_0 is the unrenormalized frequency of tunneling oscillations at $\alpha = 0$.

NRG as a “quantum impurity solver” in DMFT

As described in the lecture of Liebsch in this book, it is possible, using dynamical mean field theory (DMFT), to approximate models of correlated electrons on a lattice by a quantum impurity embedded in an effective medium (bath) which has to be determined self-consistently. For example, the Hubbard model can be mapped onto an effective Anderson impurity model with a hybridization function $\Delta(\omega)$, whose frequency dependence is unknown and needs to be determined from the DMFT self-consistency condition. This requires the impurity Green function $G_{d\sigma}$ to be identical to the local lattice Green function $G_{0\sigma} = \sum_k 1/(\omega + \mu - \varepsilon_k - \Sigma(\omega))$, where μ is the chemical potential, ε_k the dispersion relation of the lattice and $\Sigma(\omega)$ is the electron self-energy, identified as the impurity self-energy in DMFT. A highly accurate representation of $\Sigma(\omega)$ for quantum impurity models has been introduced in [29] and finds application in DMFT. Fig. 13 shows the behaviour of the $T = 0$ spectra for the Hubbard model on going through the metal-insulator transition using this approach.

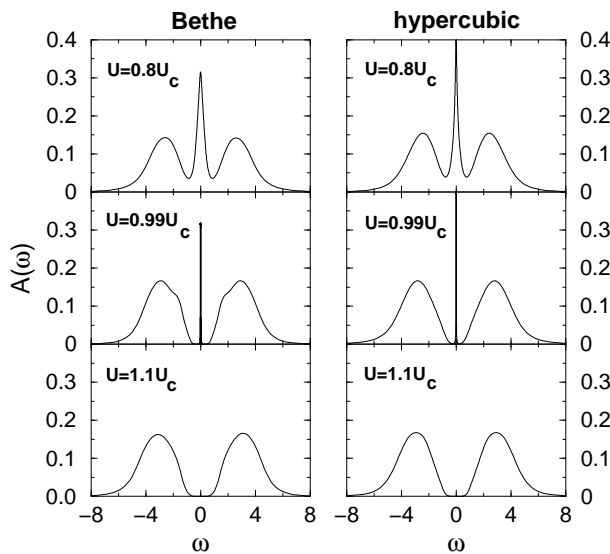


Fig. 13: Local spectral density of the Hubbard model on Bethe and hypercubic lattices showing how the $T = 0$ metal-insulator transition occurs with increasing Coulomb interaction U [25]. For $U < U_c$ the system is metallic with a quasi-particle peak at $\omega = 0$, whereas for $U > U_c$ the system is insulating with a gap between the upper and lower Hubbard bands

6 Summary

The NRG transformation for the Kondo model is a powerful tool for the study of quantum impurity models. It gives information on the many-body eigenvalues and eigenstates of such models on all energy scales and thereby allows the direct calculation of their thermodynamic, dynamic, and transport properties. Recently it has been further developed to yield the transient response of these systems to sudden perturbations for both short and long-time limits [22, 23]. The method has been extended in new directions, such as to models with bosonic baths [26] to study spin-boson models and the interplay of correlations and phonon effects in Anderson-Holstein models [27]. It has also been used successfully to make progress on understanding the Mott transition, heavy fermion behaviour and other phenomena in correlated lattice models [15, 25, 28].

There is room for further improvement and extensions of the method both technically and in the investigation of more complex systems such as multi-orbital models [30]. The use of a logarithmic discretization of the conduction band, for example, gives rise to insufficient resolution at higher energies. Approaches [17] for overcoming these difficulties are therefore of interest. The NRG also has potential to give information on the non-equilibrium transport through correlated impurity systems such as quantum dots. However, away from equilibrium, the absence of a ground state requires new criteria other than energy for eliminating unimportant states. Ideas based on the DMRG may prove useful in this respect.

Appendices

A Lanczos procedure

Neglecting spin indices, the conduction electron operator is

$$H_c = \sum_k \varepsilon_k c_k^\dagger c_k$$

The Lanczos algorithm for tridiagonalizing this operator by repeated action on the state $|0\rangle$ is

$$|1\rangle = \frac{1}{\lambda_0} [H_c|0\rangle - |0\rangle\langle 0|H_c|0\rangle] \quad (47)$$

$$|n+1\rangle = \frac{1}{\lambda_n} [H_c|n\rangle - |n\rangle\langle n|H_c|n\rangle - |n-1\rangle\langle n-1|H_c|n\rangle] \quad (48)$$

yielding

$$H_c = \sum_{n=0}^{\infty} \epsilon_n f_n^\dagger f_n + \lambda_n (f_n^\dagger f_{n+1} + H.c.) \quad (49)$$

where $\epsilon_n = \langle n|H_c|n\rangle$ and λ_n are normalizations obtained from (47-48).

B Logarithmic discretization approximation

The approximation

$$H_c = \int_{-1}^{+1} d\varepsilon \varepsilon c_{\varepsilon,\mu}^+ c_{\varepsilon,\mu} \approx \sum_{n=0}^{\infty} (\varepsilon_{-n} c_{-n,\mu}^+ c_{-n,\mu} + \varepsilon_{+n} c_{+n,\mu}^+ c_{+n,\mu}) \quad (50)$$

used to replace the continuum band in (11) by the discrete one in (14) can be analyzed by introducing a complete orthonormal basis set of states for the conduction electrons in each interval $\pm[\Lambda^{-(n+1)}, \Lambda^{-n}]$ using the following wavefunctions

$$\psi_{np}^{\pm}(\varepsilon) = \begin{cases} \frac{\Lambda^{n/2}}{(1-\Lambda^{-1})^{1/2}} e^{\pm i\omega_n p \varepsilon} & \text{for } \Lambda^{-(n+1)} < \pm\varepsilon < \Lambda^{-n} \\ 0 & \text{otherwise} \end{cases} \quad (51)$$

Here p is a Fourier harmonic index and $\omega_n = 2\pi\Lambda^n/(1 - \Lambda^{-1})$. The operators $c_{\varepsilon\sigma}$ can be expanded in terms of a complete set of new operators $a_{np\sigma}, b_{np\sigma}$ labeled by the interval n and the harmonic index p

$$c_{\varepsilon\sigma} = \sum_{np} [a_{np\sigma} \psi_{np}^+(\varepsilon) + b_{np\sigma} \psi_{np}^-(\varepsilon)]. \quad (52)$$

In terms of these operators, the Kondo Hamiltonian becomes,

$$\begin{aligned} H_{KM} &= \frac{1}{2}(1 + \Lambda^{-1}) \sum_{np} \Lambda^{-n} (a_{np\sigma}^\dagger a_{np\sigma} - b_{np\sigma}^\dagger b_{np\sigma}) \\ &+ \frac{(1 - \Lambda^{-1})}{2\pi i} \sum_n \sum_{p \neq p'} \Lambda^{-n} (a_{np\sigma}^\dagger a_{np'\sigma} - b_{np\sigma}^\dagger b_{np'\sigma}) e^{\frac{2\pi i(p-p')}{1-\Lambda^{-1}}} \\ &+ J f_{0,\mu}^+ \vec{\sigma}_{\mu\nu} f_{0,\nu} \cdot \vec{S} \end{aligned} \quad (53)$$

where in terms of the new operators, $f_{0,\mu} = \frac{1}{\sqrt{2}} \int_{-1}^{+1} d\varepsilon c_{\varepsilon,\mu}$ contains only $p = 0$ states:

$$f_{0,\mu} = \frac{1}{\sqrt{2}} \int_{-1}^{+1} d\varepsilon c_{\varepsilon,\mu} = \left[\frac{1}{2}(1 - \Lambda^{-1}) \right]^{1/2} \sum_{n=0}^{\infty} \Lambda^{-n/2} (a_{n0\mu} + b_{n0\mu}) \quad (54)$$

We notice that only the $p = 0$ harmonic appears in the local Wannier state. This is a consequence of the assumption that the Kondo exchange is independent of k . Hence the conduction electron orbitals a_{np}, b_{np} for $p \neq 0$ only couple to the impurity spin indirectly via their coupling to the a_{n0}, b_{n0} in the second term of (53). This coupling is weak, being proportional to $(1 - \Lambda^{-1})$, and vanishes in the continuum limit $\Lambda \rightarrow 1$, so these states may be expected to contribute little to the impurity properties compared to the $p = 0$ states. This is indeed the case as shown by explicit calculations in [1]. The logarithmic discretization approximation consists of neglecting conduction electron states with $p \neq 0$, resulting in H_c given by Eq. (50) with $c_{+n,\mu} \equiv a_{n,0,\mu}$ and $c_{-n,\mu} \equiv b_{n,0,\mu}$ and a discrete Kondo Hamiltonian given by Eq. (14).

References

- [1] K. G. Wilson, Rev. Mod. Phys. **47**, 773 (1975)
- [2] P. Nozières, J. Low Temp. Phys. **17**, 31 (1974)
- [3] A. C. Hewson, *The Kondo Problem to Heavy Fermions*, Cambridge University Press (1993)
- [4] P. W. Anderson, J. Phys. C **3**, 2439 (1970)
- [5] U. Weiss, *Quantum Dissipative Systems*, Series in Modern Condensed Matter Physics, Vol. 2, 2nd edition, World Scientific, Singapore (1999); A. J. Leggett, S. Chakravarty, A. T. Dorsey, M. P. A. Fisher, A. Garg and W. Zwerger, Rev. Mod. Phys. **59**,1 (1987)
- [6] W. J. de Haas, J. de Boer and G. J. van den Berg, Physica **1**, 1115 (1934).
- [7] P. W. Anderson, Phys. Rev. **124**, 41 (1961)
- [8] R. Bulla, Th. Pruschke and A. C. Hewson, J. Phys. Cond. Matt. **9**, 10463 (1997)
- [9] H. B. Krishnamurthy, J. W. Wilkins and K. G. Wilson, Phys. Rev. B **21**, 1044 (1980)
- [10] S. R. White, Phys. Rev. Lett. **69**, 2863 (1992); Phys. Rev. B **48**, 10345 (1993); Phys. Rep. **301**, 187 (1998); S. R. White and R. M. Noack, Phys. Rev. Lett. **68**, 3487 (1992)
- [11] K. G. Wilson and J. Kogut, Phys. Rep. C**12**, 75 (1974)
- [12] T. A. Costi and C. Kieffer, Phys. Rev. Lett. **76**, 1683 (1996); T. A. Costi, Phys. Rev. Lett. **80**, 1038 (1998); T. A. Costi and G. Zaránd, Phys. Rev. B **59**, 12398 (1999)
- [13] O. Sakai, Y. Shimizu and T. Kasuya, J. Phys. Soc. Jap.**58** 3666 (1989)
- [14] T. A. Costi and A. C. Hewson, Phil. Mag. B**65**, 1165 (1992); T. A. Costi, A. C. Hewson and V. Zlatić J. Phys. Condens. Matt. **6**, 2519 (1994)
- [15] R. Bulla, T. A. Costi and D. Vollhardt, Phys. Rev. B **64**, 045103 (2001)
- [16] W. Metzner and D. Vollhardt, Phys. Rev. Lett. **62**, 324 (1989); A. Georges, G. Kotliar, W. Krauth and M. J. Rozenberg, Rev. Mod. Phys. **68**, 13 (1996)
- [17] M. Yoshida, M. A. Whitaker and L. N. Oliveira, Phys. Rev. B**41**, 9403 (1990)
- [18] W. C. Oliveira and L. N. Oliveira, Phys. Rev. B**49**, 11992 (1994); S. C. Costa, C. A. Paula, V. L. Líbero and L. N. Oliveira, Phys. Rev. B**55**, 30 (1997)
- [19] T. A. Costi, Phys. Rev. Lett. **85**, 1504 (2000); Phys. Rev. B**64**, 241310 (2001)
- [20] W. Hofstetter, Phys. Rev. Lett. **85**, 1508 (2000)
- [21] D. Goldhaber-Gordon, J. Göres, M. A. Kastner, H. Shtrikman, D. Mahalu and U. Meirav, Phys. Rev. Lett. **81**, 5225 (1998)
- [22] T. A. Costi, Phys. Rev. B**55**, 3003 (1997)

-
- [23] F. Anders and A. Schiller, *Phys. Rev. Lett.* **95**, 196801 (2005)
 - [24] P. Nozières and C. T. De Domenicis, *Phys. Rev.* **178**, 1097 (1969).
 - [25] R. Bulla, *Phys. Rev. Lett.* **83**, 136 (1999)
 - [26] R. Bulla, H-Y. Lee, N-H. Tong and M. Vojta, *Rev. B* **71**, 045122 (2005)
 - [27] A. C. Hewson, D. Meyer, *J. Phys. Condens. Matter* **14**, 427 (2002).
 - [28] T. Pruschke, R. Bulla and M. Jarrell, *Phys. Rev. B* **61**, 12808 (1999); T. A. Costi and N. Manini, *J. Low Temp. Phys.* **126**, 835 (2002)
 - [29] R. Bulla and Th. Pruschke and A. C. Hewson, *J. Phys. Cond. Matt.* **10**, 8365 (1998)
 - [30] T. Pruschke and R. Bulla, *European Physical Journal B* **44**, 217 (2005)